Proc. IEEE International Conference on Biomedical Robotics and Biomechatronics (BioRob) 2014

Design of a New MR-Compatible Haptic Interface with Six Actuated Degrees of Freedom

Mehmet Alper Ergin[1], Markus Kühne[1], Axel Thielscher[2] and Angelika Peer[1]

***Abstract*— Functional magnetic resonance imaging is an often adopted tool to study human motor control mechanisms. Highly controlled experiments as required by this form of analysis can be realized with haptic interfaces. Their design is challenging because of strong safety and MR compatibility requirements. Existing MR-compatible haptic interfaces are restricted to maximum three actuated degrees of freedom. We propose an MR-compatible haptic interface with six actuated degrees of freedom to be able to study human brain mechanisms of natural pick-and-place movements including arm transport. In this work, we present its mechanical design, kinematic and dynamic model, as well as report on its model-based characterization. A novel hybrid control scheme for the employed ultrasonic motors is introduced. Preliminary MR compatibility tests based on one complete actuator-sensor module are performed. No measurable noise is found and thus, bidirectional compatibility of the six DoF interface can be expected.**

I. Introduction

Functional magnetic resonance imaging (fMRI) is an often adopted tool to study human motor control mechanisms. Highly controllable body movements are a prerequisite for this form of analysis and can be realized with the help of haptic interfaces. Haptic interfaces can provide the operator with highly standardized and easily configurable force/torque information and can read the operator's motion/force input for subsequent statistical analyses.

Imaging procedures and MR hardware, however, pose a series of challenges on the development of MR-compatible haptic interfaces: safety, bidirectional compatibility, limited device workspace and limited accessibility to this workspace, development of MR-compatible hardware as well as MR compatibility testing [1]. For definition and use of the term *MR-compatible* the interested reader may refer to [2]. MR scanners create a large static magnetic field which inevitably leads to high accelerating forces acting on ferromagnetic materials. Thus, to avoid *safety* hazards resulting from such components, devices need to be engineered from materials with low magnetic susceptibility. Further, electromechanical components need to be characterized by *bidirectional compatibility*, which means that they do not disturb the scanning process by emitting radio frequencies and causing image artifacts, but also that their functionality and performance remains unaffected by the high static magnetic field as well as the time-varying gradient fields of the MR environment. Achieving an *MR-compatible hardware* requires a careful selection of mechanical and electronic components. Further the device should undergo *MR compatibility tests* to verify both, the imaging process is not disturbed by the haptic interface and the strong magnetic field of the scanner does not affect the operation of the device.

Most state-of-the-art MR-compatible haptic interfaces are restricted to one or two degrees of freedom (DoF). In [3]–[5] input devices with one rotational or translational DoF are presented. Actuation is realized with ultrasonic, hydraulic or pneumatic actuators. In [4], induction coils, that are moved by Lorentz forces induced by the magnetic field of the MR scanner, are used for actuation. The device introduced in [6] provides resistive grasping forces by electro-rheological-fluid-based actuators. Position and torque are measured with an optical encoder and strain gauges.

Haptic devices with two DoF are proposed in [7]–[10]. A pantograph-type parallel manipulator has been developed in [7]. The device uses ultrasonic motors for power transmission and optical encoders for the position information. In [8] a device with a parallelogram mechanism, which equips pneumatic pistons for actuation and optical encoders for position sensing, is presented. The interface developed in [9] is based on a serial kinematics to achieve two DoF movements and actuated with custom-made electrostatic motors. The forces are measured with optical sensors while the position is controlled in open-loop. The device introduced in [10] uses a master-slave system with hydrostatic transmission, where only the slave is MR-compatible, to create planar movements. Positions are measured with optical encoders and forces with optical sensors.

Finally, a three DoF MR-compatible haptic interface was presented in [11], [12]. It is based on a parallel kinematics, employs DC-motors for actuation and optical encoders for position sensing. The actuators are placed two meters away from the scanner bore to avoid magnetic interference and forces are transmitted to the subject via tendons. Another three DoF MR-compatible haptic interface was proposed in our previous work [13]. The device has a parallel kinematic structure and can lead finger movements in a translational workspace. The manipulator is actuated using ultrasonic motors while optical encoders gather position information. Motor torques are measured using strain gauges.

Summarizing, state-of-the-art MR-compatible haptic interfaces are so far restricted to maximum three actuated DoF only.

[1]M. A. Ergin, M. Kühne and A. Peer are with the Institute of Automatic Control Engineering, Technische Universität München, 80333 Munich, Germany {alper.ergin, markus.kuehne, angelika.peer}@tum.de

[2]A. Thielscher is with the Biomedical Engineering Section, Danmarks Tekniske Universitet, DK-2800 Kgs. Lyngby; the Danish Research Center for Magnetic Resonance, Copenhagen University Hospital Hvidovre, DK-2650 Hvidovre; and the MPI for Biological Cybernetics, D-72012 Tübingen axel.thielscher@tuebingen.mpg.de

In this paper, we present a newly developed MR-compatible haptic interface with six actuated DoF that can be used to study human brain mechanisms of natural pick-and-place movements including arm transport. Such movements require haptic feedback via three translational and three rotational DoF, to simulate horizontal and vertical forces as well as torques that appear during manipulation of everyday objects. We will be able to render realistic pick-and-place tasks with objects of different weights and in multiple orientations. With an additional actuated DoF at the end effector, precision grasps of objects of different sizes and/or a slippery surface can be considered. Thus, we may be able to finally better treat open neuroscientific questions and to approach novel types of questions [14]. In our application, we aim to investigate complex movements, involving finger and forearm muscles, which tend to produce a strong activation within human primary motor and somatosensory cortices. Thus, we expect favorable conditions for fMRI analysis.

The newly proposed six DoF haptic interface is presented in Section II. We briefly introduce the system requirements and explain its kinematic design. Then, we describe the employed materials, actuators and sensors. Section III is devoted to the derivation of the kinematic and dynamic model. In Section IV we evaluate the performance of the developed device with respect to reachable and dexterous workspace as well as output capabilities and discuss them in light of the design requirements. Section V addresses the control of the ultrasonic motors. Preliminary MR compatibility tests are presented in Section VI. Finally, Section VII concludes the paper and provides an outlook to future work.

II. Design of a Six DoF Haptic Interface

A. Design Requirements

Design requirements of the six DoF haptic interface are identified following the terminology in [15], which distinguishes between imperative, optimal, primary and secondary requirements.

The imperative criteria are the properties that the haptic interface should satisfy in any circumstances. Safety and MR compatibility are the imperative design requirements for the proposed haptic interface. MR compatibility can be pursued through the components that do not cause artifacts in the MR image and are unaffected in their functionality and performance by the MR environment. Eliminating materials with high conductivity in the design promotes safety and allows preventing the induction of eddy currents, which may heat the material, cause skin burns and result in artifacts in the MR images. Moreover, additional velocity limiters and watchdogs can help to eliminate malfunction of the device in the appearance of undesired control signals.

Optimal criteria, on the other hand, define performance measures the mechanism is optimized for. Optimal requirement is the *minimum footprint*, since the mechanism needs to be compact enough to fit inside the scanner bore, which can have a diameter ranging from 500 mm up to 700 mm.

The primary criteria encapsulate the properties which are aspired initially and appear in design specifications, but can be modified if required. Primary criteria for the six DoF haptic interface are the workspace dimensions as well as force, torque and velocity output capabilities. Despite of the rather large range of motion of the human arm, its practical *workspace* is quite restricted inside the MR scanner, since the shoulder as well as the upper arm are fixed in order to not cause image artifacts. As a result, the workspace of the device can be approximately restricted to the workspace of the human wrist and hand. According to the ASSH guidelines [16], the human wrist has a workspace of 70° of extension, 75° of flexion, 20° of radial deviation and 35° of ulnar deviation. As in the envisaged pick-and-place tasks the wrist has negligible amount of extension, we decided to only consider wrist flexion as design requirement. The translational workspace of the hand is derived following the kinematics proposed in [17] and is approximated as half ellipsoid with 34.5 mm x 47 mm x 46 mm semi principle axes.

In terms of output capability, psychophysical experiments suggest that velocities up to 1 m/s and accelerations up to 9.81 m/s^2 are required for haptic rendering [18]. The maximum required forces and torques to move the rendered objects are limited to 2 N and 0.05 Nm. This allows pick-and-place simulations of light objects.

Finally, secondary criteria are not considered in the specifications, but allow to achieve imperative, optimal and primary criteria while choosing between multiple design solutions. Secondary design requirements for the device are identified as *low friction, backlash, and weight*.

B. Kinematic Design

Robotic manipulators can be designed with either parallel, serial or hybrid kinematics. Parallel kinematics are typically characterized by a low inertia as actuators can be positioned in the base and thus, exhibit a higher bandwidth than their serial kinematics counterparts. Parallel kinematics are furthermore known for their rather high stiffness, which can hardly be achieved by serial kinematics. Finally, parallel kinematics allow the combination of actuator power on top of a very compact design. As a consequence, parallel mechanisms have been often selected as the underlying kinematics of six DoF haptic interfaces [19]–[21].

Beside these advantages that lead to a better haptic rendering performance, parallel kinematics also bear advantages for the design of MR-compatible haptic interfaces. MR-compatible materials usually suffer from low rigidity, which can be partially compensated by a parallel kinematics. Moreover, in parallel kinematics actuators and sensors can be easily installed in the base, which helps to reduce image artifacts. In serial kinematics, on the other hand, actuators and sensors would move during operation and thus, emitted radio frequencies would interfere with the scanning process.

Based on these considerations we decided to base our design on the 6-RSS parallel kinematics proposed in [22], but in order to decrease joint complexity while maintaining compactness and simultaneously increasing rotational workspace, we decided to use revolute joints instead of spherical ones

resulting in a 6-RRRRRR design. A non-MR-compatible prototype with the same kinematics was proposed in our previous work [23].

The CAD model of the proposed kinematics can be seen in Figure 1.

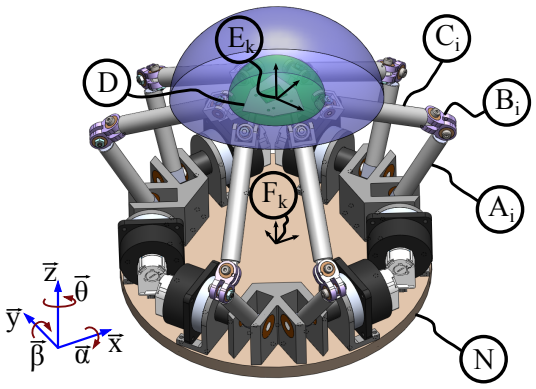

Fig. 1: Frames F_k (k = 1,2,3), located on the Newtonian body N, are rotated about 120° against each other and form the symmetry axis for each of the neighbouring, actuated bodies A_i (i = 1,2,...,6). Via rotary joints and bodies B_i and C_i those are connected to the end effector D with frames E_k. The blue and green half ellipsoids are the visualisations of the reachable and the dexterous workspaces respectively.

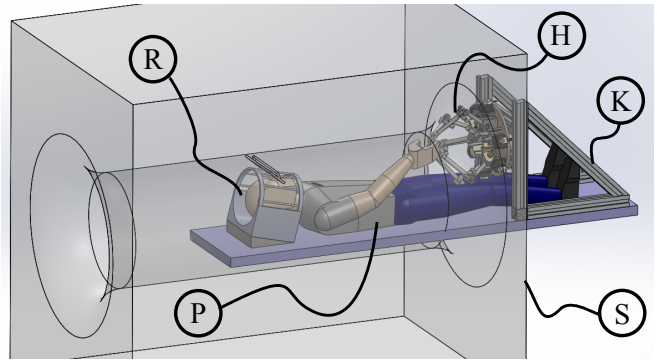

Fig. 2: The proposed six DoF haptic interface H mounted on a support frame K at the entry of the bore of the scanner S. The head of subject P is fixed in a head restraint R.

The employed modified gimbal mechanism covers larger rotations at the trade-off of a larger footprint, compared to spherical joints. Considering the required workspace, link lengths have been identified as follows: 125 mm, 175 mm and 21 mm for lower, upper and offset links, respectively. The round base, denoted as Newtonian body N, has a diameter of 360 mm and will be mounted vertically at the entry of the scanner bore. Thus the subject's hand is directly in the line of sight to provide congruence between visual and haptic information. The position of the haptic device H in front of the scanner S, manipulated by a subject P is shown in Figure 2. Depicted is also a support frame K for the haptic interface, which is attached to the scanner bed. A head restraint system R fixes the head to avoid artifacts due to head movement. The head restraint system R has been slightly inclined for the experiments.

C. Implementation

In contrast to traditional haptic interfaces the variety of materials, actuators and sensors is strongly restricted due to safety and MR compatibility requirements.

a) Materials: The choice of materials is handled considering the imperative design criteria described in Section II-A. The design of the newly developed haptic interface uses materials like rigid PVC, ABS+ (Acrylnitril-Butadien-Styrol), nylon, and glass. Rotary joints are realized employing xiros polymer ball bearings that contain glass-balls and are manufactured by igus. Unlike high precision steel bearings, they impose backlash due to manufacturing tolerances. Thus, to prevent backlash, nylon shoulder screws and nuts are employed. Upper and lower links of the device are of glass-fiber to achieve both, high rigidity and low electrical conductivity.

b) Actuators and Sensors: Similar to the choice of construction materials, also the choice of actuators and sensors is limited. State-of-the-art, MR-compatible haptic interfaces use pneumatic, hydraulic, electrostatic or piezoelectric actuators, stepping motors, ultrasonic motors or electroactive polymers. Each of these actuation principles comes along with certain advantages and disadvantages [13]. In this work, ultrasonic motors of type Shinsei USR60 with 0.5 Nm output torque were selected since they can be produced using non-ferromagnetic materials, enable rotational movements, output high torques and have good velocity control characteristics on top of a compact design. The position is obtained from Avago HEDM-5540-B14 optical encoders, which are built in with the ultrasonic motors and have a resolution of 1000 counts per revolution. Force sensing is realized using strain-gauge-based torque sensors of type ME-Systeme TS-70 with a measurement range of 2 Nm, a stiffness of 1000 Nm/rad and a bandwidth of 5 kHz. The sensor-frame is machined from aluminium and the amplifying circuit is shielded with a copper housing. Shielded twisted-pair cables are employed to carry the sensor signals.

III. Kinematic and Dynamic Model

For the proposed 6-RRRRRR mechanism no analytical forward or inverse kinematic solution exists. Thus, in this study we derived solutions for inverse and forward kinematics with numerical methods. In order to formulate the kinematics problems we defined six closed loop kinematic chains as shown in Figure 3:

$$\mathbf{0} = \mathbf{os} + \mathbf{sp} + \mathbf{pt} + \mathbf{tv} + \mathbf{vy} + \mathbf{yz} + \mathbf{ze} + \mathbf{eo}. \quad (1)$$

Equation 1 yields the exemplified formation of a closed kinematic chain as depicted in Figure 3. Points p, t, v and y are located at the center of rotational joints. Vectors **os** and **sp** are fixed in the Newtonian body N while **pt** is co-linear to A_i. Vectors **tv** and **vy** are co-linear to B_i and C_i respectively. The link from the tip of C_i to the center of the end effector D is defined by vectors **yz** and **ze**. The kinematic chain is closed with vector **os**, which starts at the center of D and ends at the center of N.

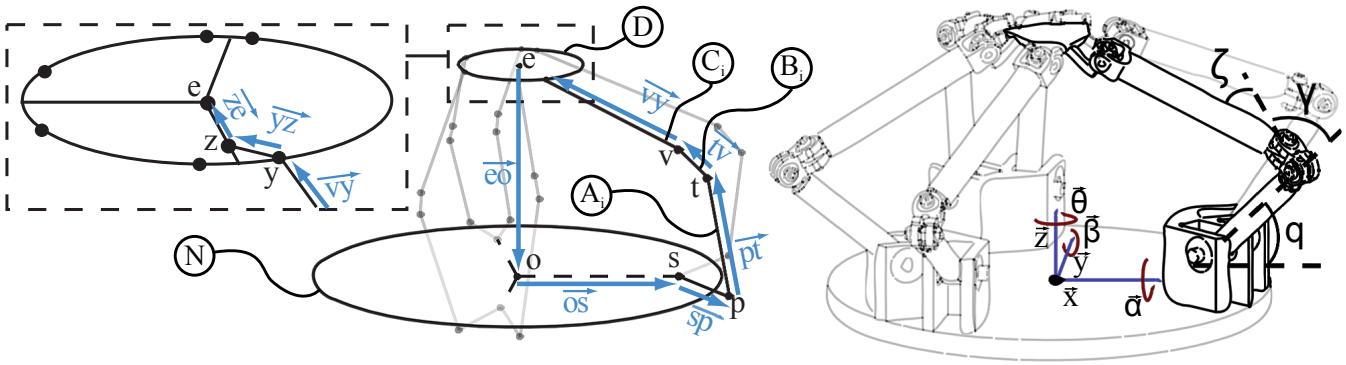

Fig. 3: Left: visualizes an example of a closed loop equations to derive the solutions for inverse and forward kinematics. In order to formulate the kinematics problem we defined six closed loop kinematic chains along the bodies A_i, B_i, C_i and D. Right: angular and translational variables of the mechanism are illustrated along the specified coordinate axis.

Similar to the example in Equation 1, six loop vectors are defined in all three components of the Cartesian coordinate system, x, y and z and as a result we get 18 independent equations. Required variables are shown in Figure 3, where q_i are the actuated angles, γ_i the angles between lower link and offset element, ζ_i the angles between the offset element and the upper links, x, y and z the end effector positions and α, β and θ the end effector rotations. In total there are 24 variables. For the inverse kinematics problem six of these variables (end effector rotations and positions) are known in advance. As a result, 18 unknowns remain and can be derived by solving 18 loop equations using iterative methods. Here a modified version of the Kutta-Merson algorithm is employed. Similarly, for the forward kinematics problem the actuated joint angles are pre-defined and the end effector positions can be derived by iterating the coefficient matrix.

The dynamic analysis of the proposed haptic interface requires the differentiation of the loop equations. Using these derivatives, generalized velocities and accelerations can be determined that are required to form the dynamic equations in Kane's method [24]. The inertial parameters of the mechanism are obtained from the CAD model realized in Solidworks. Since both kinematic and dynamic equations have no analytic solution, they are formed symbolically in Autolev and are embedded into Matlab/Simulink where they are solved numerically in real-time. Thus, they cannot be yielded explicitly.

IV. Model-based Characterization

In this section, a model-based characterization of the proposed MR-compatible haptic interface will be performed considering reachable workspace, dexterous workspace and output capabilities.

A. Reachable Workspace

The reachable workspace is defined as "the region the end effector frame can reach with at least one orientation" [25]. The reachable workspace is found as follows: A set of end effector positions and rotations defined in Cartesian space are passed as inputs to the inverse kinematics. If the numerical solver reaches a solution, we check whether joint limits are satisfied. The reachable workspace of the proposed haptic interface is identified as a half ellipsoid with $a = 110$ mm, $b = 110$ mm, $c = 75$ mm semi-principle axes and a rotational workspace of 120° in α and β directions as well as 180° in θ direction. It is depicted in Figure 1 as blue volume.

B. Output Capability and Dexterous Workspace

Output capability is one of the most widely accepted performance measures used for the characterization of haptic interfaces. In this work output capabilities are studied for force, velocity, and acceleration with the help of the previously determined kinematic and dynamic models. The evaluation is based on the method proposed in [26]. The algorithm transforms the analysis into an optimization problem in order to find the direction of the minimum of the maximum output vector at a given point in the workspace. The velocity, force/torque and acceleration outputs are defined as follows:

$$\begin{pmatrix} \dot{\boldsymbol{x}} \\ \boldsymbol{\omega} \end{pmatrix} = \boldsymbol{J}(\boldsymbol{q})\dot{\boldsymbol{q}} \tag{2}$$

$$\boldsymbol{h} = (\boldsymbol{J}(\boldsymbol{q})^{-1})^T \boldsymbol{\tau}; \qquad \dot{\boldsymbol{q}} = \boldsymbol{0} \tag{3}$$

$$\begin{pmatrix} \ddot{\boldsymbol{x}} \\ \dot{\boldsymbol{\omega}} \end{pmatrix} = \boldsymbol{J}(\boldsymbol{q})\boldsymbol{M}^{-1}\boldsymbol{\tau}; \qquad \dot{\boldsymbol{q}}, \boldsymbol{h} = \boldsymbol{0} \tag{4}$$

where $\dot{\boldsymbol{x}}$ and $\boldsymbol{\omega}$ are the translational and angular velocities of the end effector, $\boldsymbol{J}(\boldsymbol{q})$ is the Jacobian, $\boldsymbol{h}$ represents forces and torques applied at the end effector, $\boldsymbol{\tau}$ is the motor torque, $\ddot{\boldsymbol{x}}$ and $\dot{\boldsymbol{\omega}}$ are the translational and rotational output accelerations, and $\boldsymbol{M}$ is the mass matrix of the mechanism.

To provide some insight into the shape of the output capability hypersurfaces, Figure 4 illustrates the minimum of the maximum velocity, force and acceleration output capability that can be achieved at $z = 175$ mm for all rotational configurations, which is around the middle of the workspace for the z-coordinate.

In order to determine characteristic values for the output capability of the device, the dexterous workspace has to be defined first. The dexterous workspace is a subset of the reachable workspace and is defined as "the region the end effector frame can describe while attaining different orientations" [25]. We determined the dexterous workspace by inspecting the force, velocity and acceleration output

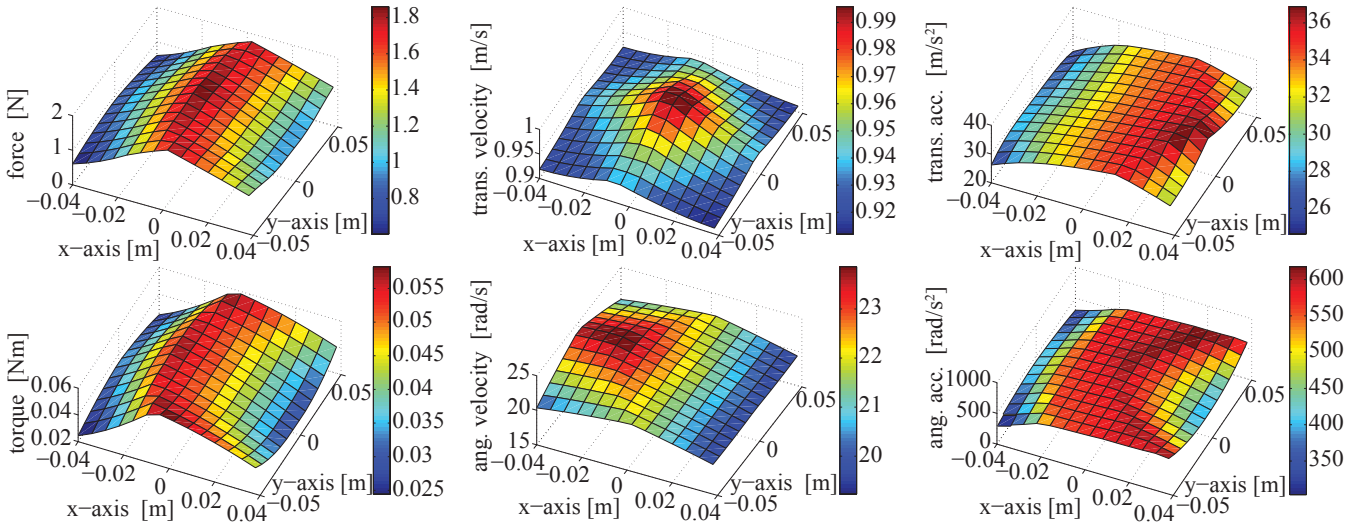

Fig. 4: Minimum of the maximum velocities, forces/torques and accelerations evaluated over the reachable workspace at $z = 175$ mm.

capabilities of the mechanism. As can be seen in Figure 4 the output capability decreases rapidly at the edges of the hyperplanes. Correspondingly, the dexterous workspace was chosen to exclude these extreme points. The shape of the dexterous workspace, depicted in Figure 1 as green volume, was finally decided to be a half ellipsoid with $a = 40$ mm, $b = 50$ mm, $c = 50$ mm semi-principle axes on x, y and z directions and can be reached from all sides assuming the subject is in supine position inside the scanner and the z-axis of the device points to the inside of the scanner bore, while the x-axis points towards the ceiling of the room. In this configuration, the radial and ulnar deviation of the wrist create a rotary movement about the y-axis of $\beta = 55°$, while the wrist flexion exerts a rotation about the x-axis of $\theta = 75°$.

Given this dexterous workspace, the minimum and maximum values of the output capabilities are derived using the kinematic and dynamic model of the haptic interface over the entire dexterous workspace and are listed in Table I.

TABLE I: Output capabilities are determined using the model of the device over the whole dexterous workspace assuming manipulations in all 6 DoF

	Continuous Forces/Torques		Continuous Velocities		Continuous Accelerations	
	Min.	Max.	Min.	Max.	Min.	Max.
Linear	0.65 [N]	2.6 [N]	0.75 [m/s]	1.15 [m/s]	23.8 [m/s^2]	37.1 [m/s^2]
Angular	0.025 [Nm]	0.07 [Nm]	18.7 [rad/s]	23.9 [rad/s]	281 [rad/s^2]	653 [rad/s^2]

Inside the dexterous workspace the minimum of the maximum velocity was found to be 0.75 m/s. This number is close to the maximum required velocity, which was identified in Section II-A. Based on human psychophysical experiments, a maximum of 9.81 m/s^2 acceleration capability is required for a high performance haptic rendering [18] and the proposed interface can reach at least 23.8 m/s^2 in worst case. The minimum of the maximum force and torque output capabilities of the proposed device are found to be 0.65 N and 0.025 Nm at the limits of the workspace. So despite of the very good performance in terms of velocity and acceleration output capabilities, continuous force and torque output capabilities decrease drastically when being forced to simultaneously realize large rotations about all three axes and thus, future designs have to face this problem.

V. Control

Simulating virtual environments and rendering interaction forces between haptic interface and operator can be realized by two complementary control paradigms: Impedance control, where positions are measured to control the desired interaction force and admittance control, where forces or torques are measured and the motion of the device is controlled. Admittance control can compensate for non-linearities and is well suited for the interaction of the device with low impedances.

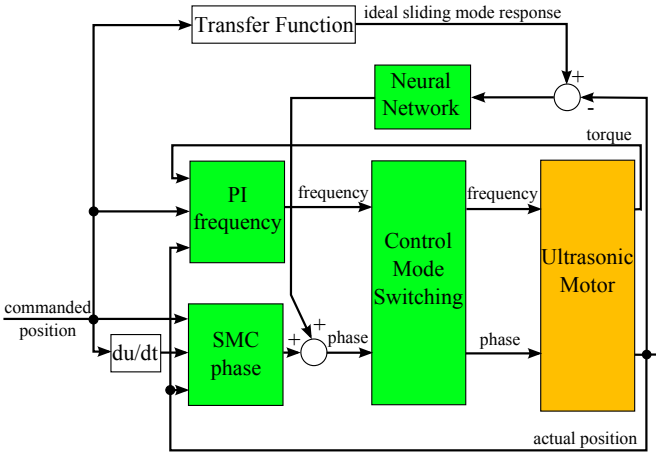

Fig. 5: Control scheme of the hybrid controller for the ultrasonic motor, switching between phase and frequency control.

In order to implement admittance control for the haptic device, the ultrasonic motors have to be position-controlled. But non-linearities appear when load is added to the rotor and therefore the use of linear control techniques, like standard PI control, is difficult.

Ultrasonic motors can be driven by control of frequency and phase differences. At low velocities and under load, which is one of the most relevant situations to be considered for haptic devices, frequency control suffers from dead-zones and stick-slip phenomena. It is, however, well suited for motion control at high velocities. Adopting phase control, on the other hand, high velocities cannot be reached, but it allows to achieve smooth movements at low velocities.

Thus, we propose a hybrid control scheme that switches between frequency and phase control to exploit advantages of both. Phase control is realized by non-linear sliding mode control, whereas frequency control is achieved with a simple PI controller. Additionally, a combination of phase dead-zone compensation techniques in form of a neural network and a mathematical model, which models the dead-zone width was adopted. The control scheme is depicted in Figure 5.

A more detailed description of the control scheme is beyond the scope of this paper and will be detailed elsewhere.

VI. MR COMPATIBILITY TESTS

Preliminary MR compatibility tests were performed for one complete, controlled actuator-sensor module, encompassing all relevant components that could interfere in an MR environment: ultrasonic motor, optical encoder, torque sensor, amplifier, and link. The control hardware is placed in the controller room while the actuator-sensor module is located in the scanner room. Amplifiers and haptic interface are connected with shielded twisted pair cables. The tests were conducted on a 3T Siemens TIM Trio scanner (Siemens Medical Solutions, Erlangen, Germany) equipped with a 12-channel head coil. The module was placed centrally and directly in front of the scanner bore, where the field strength was measured to be $\geq$ 1.26 T. We investigated if fluctuations are induced in the magnetic field or if the device function is affected. Thus, we compared scans of the powered and the unplugged module.

A. Methods

1) RF Noise Measurements: A doped spherical agar phantom and the Siemens RF noise service sequence were used to test for putative radio frequency noise transmitted by the actuator-sensor module. During a 6 min sequence, the MR gradients and RF excitation were kept switched off while the RF receiver scanned for RF noise in a range of $\pm$250 kHz relative to the center frequency at the highest possible sensitivity. The end effector of the actuator-sensor module moved with a sinusoidal velocity profile in inner and outer direction of the scanner bore at a frequency of 2 Hz. For control, a further measurement was made with the module unplugged.

2) EPI Quality Assessment: In order to test whether the module exerted any impact on echo planar images (EPI) as usually acquired during functional MRI studies of the brain we assessed whether the mean signal intensity or the temporal stability of EPI time series were affected by movements of the module. Changes in mean intensity would hint towards systematic effects on the static magnetic field, caused, e.g. by an overall increased current flow in the motors during movement phases. Even small systematic differences would bias the results of an fMRI analysis, as the latter is based on the detection of rather subtle ($\leq 1-2\%$) changes in voxel intensity (see, e.g. [27] for a similar effect). In a similar vein, AC currents in the motors during movement phases could potentially affect the temporal stability of the EPIs. As the significance of brain activations is assessed relative to the residual variance of the EPI time series, differences in the temporal stability during movement and rest-phases would again affect the fMRI results.

The first test was based on the procedures outlined in the Function Biomedical Informatics Research Network (fBIRN; [28]) protocol. Gradient echo EPI time-series images of the spherical agar phantom were acquired (200 volumes, 28 transversal slices, voxel size = 3.44x3.44x4 mm^3, 1 mm gap, matrix size = 64x64, TR/TE = 2000/30 ms, bandwidth = 1565 Hz/pixel) while the movement of the module was controlled in an ON-OFF block design: ON-blocks of 30 s during which the module moved sinusoidally at a frequency of 2 Hz were alternated with OFF-blocks of 30 s without movement. The EPI volumes corresponding to ON- and OFF-blocks were analyzed separately and the results were compared. The mean images across volumes were determined for both groups of EPIs and the difference between the mean images were taken. As further measure, the signal-to-fluctuation-noise ratio (SFNR) was determined by dividing the mean by the standard deviation across volumes, and the SFNR images of both groups of EPIs were again subtracted from each other. Lower SFNR values during the ON-blocks would indicate a higher temporal variability of the EPI signal.

As second test, a standard fMRI analysis based on the General Linear Model (GLM) was applied to the EPI data (using FSL3.3, FMRIB, Oxford University, UK). The EPI time series was temporally high-pass filtered (cutoff 120 s), spatially smoothed (Gaussian with 4 mm FWHM) and subjected to the GLM analysis. The statistical model consisted of one regressor to model the succession of ON- and OFF-blocks. The resulting statistical maps were thresholded leniently at p = 0.05 voxel level (no cluster level) to be sensitive to even small effects caused by movements of the actuator-sensor module. For control, the GLM analysis was repeated using a further EPI time-series acquired with identical parameters, but with the module unplugged.

3) Induced Voltage Measurements: Finally, we also tested whether the EPI sequence induced strong voltages in the components of the actuator-sensor module or the cables connecting it to the control computer outside the MR cabin. The cables of the encoder as well as the torque sensor were connected to an oscilloscope and signals were analyzed for induced disturbances.

B. Results

1) RF Noise and EPI Quality: Movements of the module did not induce any additional RF noise, when comparing the noise spectra for the module moving and unplugged. Visual inspection of the mean images and the corresponding

difference image did not reveal any systematic variation between the ON- and OFF-blocks, see Fig. 6. The mean signal intensities were very similar and the difference, averaged across all voxels in the phantom, was negligible ($-0.01\% \pm 0.05\%SD$).

The images showed the usual, randomly distributed thermal noise floor without any hints of systematic noise sources at one or more distinct frequencies. In other words, the noise with the device in place was identical to the situation which is observed when having usually only the phantom in place. As no noise could be detected in the first instance, the measurement was not repeated without the device in place, as no additional knowledge gain was to be expected from that.

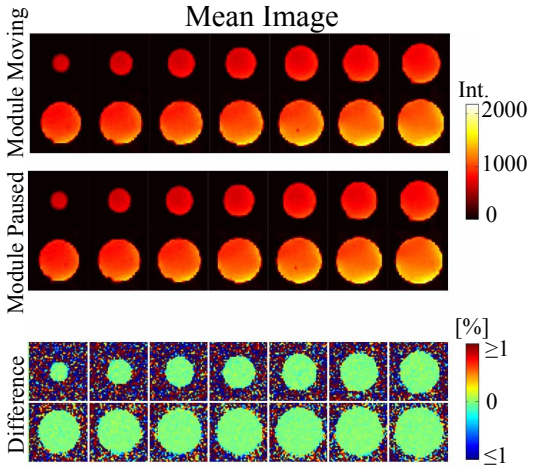

Fig. 6: Mean images for the EPIs acquired during the ON- and OFF-blocks and difference image. The first 14 out of 28 slices are shown.

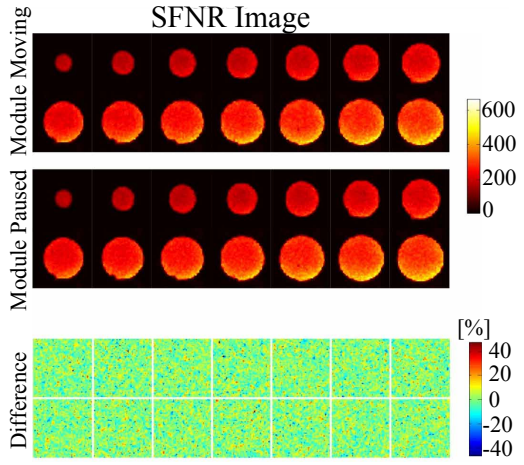

Fig. 7: SFNR images for the ON-and OFF-blocks and corresponding difference image.

Comparable results were obtained for the SFNR images, see Fig. 7. Even though the difference varied up to $\pm 45\%$ on a voxel-to-voxel basis, the variations were randomly distributed across the difference image and did not hint towards any image region or spatial cluster with systematically

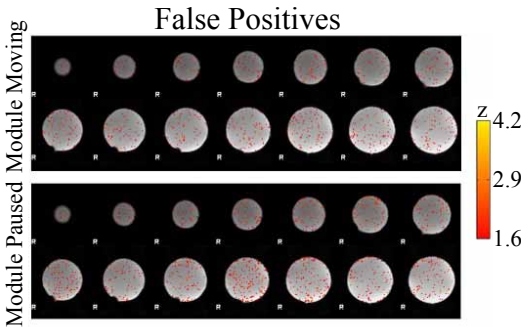

Fig. 8: Results of the GLM analysis used to compare the EPIs acquired during ON- and OFF-blocks (upper half), and corresponding control analysis with the actuator-sensor module unplugged (lower half). The absence of false positives in the background region is due to an automatic masking produce applied during analysis.

increased or decreased SFNR values. Correspondingly, the average SFNR difference across all voxels in the phantom was very small ($0.5\% \pm 10\%SD$). The movements of the haptic display did also not exert any impact on the results of the GLM analysis (upper half of Figure 8). Effects on the B_0 field origin from having the device in place or not can be easily compensated by the initial shimming procedure. Thus, no test without the device in place was performed. The number of false positive activations (5.2% of the overall voxels in the phantom) fitted to the threshold level of p = 0.05. In addition, the false positive activations were randomly distributed across the phantom, and comparable to the results obtained with the haptic display unplugged (lower half of Figure 8). To summarize, our tests demonstrate that the EPI image acquisition was not influenced by the actuator-sensor module.

2) Impact of MR Imaging on Actuator-Sensor Module: With 1V peak-to-peak, the maximal voltage induced by the EPI sequence in the motors, sensors and cables was found to be low enough to not affect any of the components of the module or the control computer. Logging the input data of the DAC card revealed no effects of the EPI sequence on the signal of the encoder. Small artifacts initially arose on the voltage signals of the torque sensor, but were then eliminated employing noise suppression chokes and capacities.

VII. Conclusion

Functional magnetic resonance imaging is an often adopted tool to study human motor control mechanisms. Highly controlled experiments can be realized with the help of haptic interfaces, but their design is challenging because of strong safety and MR compatibility requirements. While state-of-the-art devices are limited to maximum three actuated DoF we developed a new MR-compatible haptic interface with six actuated DoF to study human brain mechanisms of natural pick-and-place movements including arm transport. A parallel mechanism was selected to enable grounding of the actuators and sensors while preserving high stiffness and output capabilities. The choice of a 6-RRRRRR

kinematics allowed to significantly increase the rotational workspace compared to other known six DoF parallel kinematic designs. Materials, sensors and actuators were chosen to guarantee safety and bidirectional MR compatibility. Kinematic and dynamic models of the device were derived using symbolic methods and the device was characterized in terms of its reachable workspace, dexterous workspace and output capability. A novel hybrid control scheme for the employed ultrasonic motors was introduced and finally preliminary MR compatibility tests were conducted for one actuator-sensor module. No measurable noise was detected at all. Thus, we expect to meet acceptable noise levels for the full setup to guarantee bidirectional MR compatibility.

Future work will be directed towards further optimization of the design especially in terms of workspace size and an extension of the end effector to support precision grasps. It will also include an advancement of the control strategy and an experimental characterization of the device, in particular regarding static and dynamic friction. Finally, MR compatibility tests with the six DoF haptic interface will be carried out.

ACKNOWLEDGEMENT

This work was supported in part by the German Research Foundation (DFG) within the project "VR system for visuohaptic stimulation in the context of fMRI analyses". We would like to thank Stefan Klare for his valuable support in the preparation of the MR compatibility tests.

REFERENCES

[1] R. Gassert, E. Burdet, and K. Chinzei. Opportunities and challenges in mr-compatible robotics. *Engineering in Medicine and Biology Magazine, IEEE*, 27(3):15 –22, may-june 2008.

[2] R. Gassert, E. Burdet, and K. Chinzei. MRI-Compatible Robotics. *Engineering in Medicine and Biology Magazine, IEEE*, 27(3):12–14, may-june 2008.

[3] M. Flueckiger, M. Bullo, D. Chapuis, R. Gassert, and Y. Perriard. fmri compatible haptic interface actuated with traveling wave ultrasonic motor. In *Industry Applications Conference, 2005. Fourtieth IAS Annual Meeting. Conference Record of the 2005*, volume 3, pages 2075 – 2082 Vol. 3, oct. 2005.

[4] R. Riener, T. Villgrattner, R. Kleiser, T. Nef, and S. Kollias. fmri-compatible electromagnetic haptic interface. In *Engineering in Medicine and Biology Society, 2005. IEEE-EMBS 2005. 27th Annual International Conference of the*, pages 7024 –7027, jan. 2005.

[5] Ningbo Yu, Christoph Hollnagel, Armin Blickenstorfer, Spyros Sreejanth Kollias, and Robert Riener. fmri-compatible robotic interfaces with fluidic actuation. In *Robotics: Science and Systems*. The MIT Press, 2008.

[6] Azadeh Khanicheh, Andrew Muto, Christina Triantafyllou, Brian Weinberg, Loukas Astrakas, Aria Tzika, and Constantinos Mavroidis. fmri-compatible rehabilitation hand device. *Journal of NeuroEngineering and Rehabilitation*, 3:1–11, 2006.

[7] J. Izawa, T. Shimizu, T. Aodai, T. Kondo, H. Gomi, S. Toyama, and K. Ito. Mr compatible manipulandum with ultrasonic motor for fmri studies. In *Robotics and Automation, 2006. ICRA 2006. Proceedings 2006 IEEE International Conference on*, pages 3850 –3854, may 2006.

[8] Jörn Diedrichsen, Yasmin Hashambhoy, Tushar Rane, and Reza Shadmehr. Neural correlates of reach errors. *The Journal of Neuroscience*, 25(43):9919–9931, 2005.

[9] M. Hara, G. Matthey, A. Yamamoto, D. Chapuis, R. Gassert, H. Bleuler, and T. Higuchi. Development of a 2-dof electrostatic haptic joystick for mri/fmri applications. In *Robotics and Automation, 2009. ICRA '09. IEEE International Conference on*, pages 1479 –1484, may 2009.

[10] R. Gassert, L. Dovat, O. Lambercy, Y. Ruffieux, D. Chapuis, G. Ganesh, E. Burdet, and H. Bleuler. A 2-dof fmri compatible haptic interface to investigate the neural control of arm movements. In *Robotics and Automation, 2006. ICRA 2006. Proceedings 2006 IEEE International Conference on*, pages 3825 –3831, may 2006.

[11] Siqiao Li, A. Frisoli, L. Borelli, M. Bergamasco, M. Raabe, and M.W. Greenlee. Design of a new fmri compatible haptic interface. In *EuroHaptics conference, 2009 and Symposium on Haptic Interfaces for Virtual Environment and Teleoperator Systems. World Haptics 2009. Third Joint*, pages 535 –540, march 2009.

[12] Siqiao Li, Antonio Frisoli, Massimiliano Solazzi, and Massimo Bergamasco. Mechanical design and optimization of a novel fmri compatible haptic manipulator. In *RO-MAN*. IEEE, 2010.

[13] Stefan Klare, Angelika Peer, and Martin Buss. Development of a 3 dof mr-compatible haptic interface for pointing and reaching movements. In *Haptics: Generating and Perceiving Tangible Sensations*, volume 6192 of *Lecture Notes in Computer Science*, pages 211–218. Springer Berlin Heidelberg, 2010.

[14] Jody C Culham, Cristiana Cavina-Pratesi, and Anthony Singhal. The role of parietal cortex in visuomotor control: what have we learned from neuroimaging? *Neuropsychologia*, 44(13):2668–84, January 2006.

[15] J.-P. Merlet. *Parallel Robots*. Springer, 2006.

[16] American society for surgery of the hand, normal range of motion reference values. `http://www.assh.org/Public/HandAnatomy/Anatomy/Pages/Normal-Range-Motion.aspx`.

[17] Karim Abdel-Malek, Jingzhou Yang, Richard Brand, and Emad Tanbour. Towards understanding the workspace of human limbs. *Ergonomics*, 47(13):1386–1405, 2004. PMID: 15513715.

[18] P. Fischer, R. Daniel, and K.V. Siva. Specification and design of input devices for teleoperation. In *Robotics and Automation, 1990. Proceedings., 1990 IEEE International Conference on*, pages 540 – 545 vol.1, may 1990.

[19] E.L. Faulring, J.E. Colgate, and M.A. Peshkin. A high performance 6-dof haptic cobot. In *Robotics and Automation, 2004. Proceedings. ICRA '04. 2004 IEEE International Conference on*, volume 2, pages 1980 – 1985 Vol.2, 26-may 1, 2004.

[20] F. Gosselin, J.-P. Martins, C. Bidard, C. Andriot, and J. Brisset. Design of a new parallel haptic device for desktop applications. In *Eurohaptics Conference, 2005 and Symposium on Haptic Interfaces for Virtual Environment and Teleoperator Systems, 2005. World Haptics 2005. First Joint*, pages 189 – 194, march 2005.

[21] Sung-Uk Lee and Seungho Kim. Analysis and optimal design of a new 6 dof parallel type haptic device. In *Intelligent Robots and Systems, 2006 IEEE/RSJ International Conference on*, pages 460 –465, oct. 2006.

[22] T. Arai, H. Funabashi, Y. Nakamura, Y. Takeda, and Y. Koseki. High speed and high precision parallel mechanism. In *Intelligent Robots and Systems, 1997. IROS '97., Proceedings of the 1997 IEEE/RSJ International Conference on*, volume 3, pages 1624 –1629 vol.3, sep 1997.

[23] Mehmet Alper Ergin and Angelika Peer. Development of a new 6 DOF parallel haptic interface for the rendering of elements and interior equipment in a car. In *2013 IEEE Ro-Man*, pages 238–244. IEEE, August 2013.

[24] *Spacecraft Dynamics*. McGraw Hill, 1983.

[25] L. Sciavicco and B. Siciliano. *Modelling and control of robot manipulators*. Springer, 2001.

[26] Marc Ueberle. *Design, Control, and Evaluation of a Family of Kinesthetic Haptic Interfaces*. PhD thesis, TU München, 2006.

[27] N. Weiskopf, O. Josephs, C.C. Ruff, F. Blankenburg, E. Featherstone, A. Thomas, S. Bestmann, J. Driver, and R. Deichmann. Image artifacts in concurrent transcranial magnetic stimulation (TMS) and fMRI caused by leakage-currents: modeling and compensation. *Journal of Magnetic Resonance in Imaging*, 29(5):1211–1217, 2009.

[28] L. Friedman and G.H. Glover. Report on a multicenter fmri quality assurance protocol. *Journal of Magnetic Resonance in Imaging*, 23:827–839, 2006.